Catalysis Today 164 (2011) 268–274

Contents lists available at ScienceDirect

Catalysis Today

journal homepage: www.elsevier.com/locate/cattod

Carbon deposition on bimetallic Co–Ni/Al_2O_3 catalyst during steam reforming of glycerol

Chin Kui Cheng, Say Yei Foo, Adesoji A. Adesina *

Reactor Engineering & Technology Group, School of Chemical Engineering, The University of New South Wales, Anzac Parade, Kensington, Sydney, NSW 2052, Australia

ARTICLE INFO

Article history:
Available online 3 November 2010

Keywords:
Carbon deposition
Catalyst deactivation
Glycerol
Steam reforming

ABSTRACT

This paper reports the nature and kinetics of carbon deposition on bimetallic Co–Ni/Al_2O_3 catalyst during the steam reforming of glycerol. Reaction runs were carried out under stoichiometrically excess steam conditions between 773 and 823 K. Total organic carbon content of used catalysts varied between 18 and 30 wt.%. Carbon deposition occurred on the calcined Al_2O_3 support probably due to the presence of weak acid centres. Thermogravimetric analysis revealed two types of carbonaceous pools on catalyst surface—a relatively smaller deposit reactive with both H_2 and O_2 and a larger reservoir that could only be gasified with O_2. Gas composition analysis showed that only CH_4 and H_2O were produced during H_2-TPR while CO_2 and H_2O were produced during TPO. FTIR characterisation confirmed the presence of C–O, C–C, C–H, O–H and C=C bonds in the carbon residue. Carbon deposition rate has an order of 0.55 with respect to glycerol partial pressure and order of −0.22 for steam. Indeed, a Langmuir–Hinshelwood kinetic model involving dissociative adsorption of glycerol and molecular chemisorption of steam adequately captured the carbon deposition rate behaviour. Catalyst regeneration using a TPO–TPR–TPO–TPR scheme restored the physicochemical properties to the same level as the fresh catalyst.

1. Introduction

Coke deposition is one of the most common causes of catalyst deactivation in hydrocarbon-mediated reactions. The nature of the deposited carbon and its removal kinetics have been the subject of much inquiry in hydrocarbon-related operations [1–5]. These studies revealed that dissociative chemisorption of the hydrocarbon substrate produced surface atomic carbon or C_yH_{1-y} species (C_α species) which may undergo further dehydropolymerization on the catalyst surface to form amorphous film (C_β) with further aging leading to graphitic carbon. In some cases, it has been shown that these carbon atoms also dissolved and diffused through the metal to active growth areas such as grain boundaries where precipitation took place to form amorphous vermicular (or whisker) carbon (C_γ). This diffusion/precipitation step is possible with metals that can dissolve the carbon atoms to form carbides, such as Ni and Co metals. Under severe and prolonged reaction conditions, the amorphous carbon may be further converted into graphitic carbon (C_δ). Various techniques had been explored to evaluate the characteristics of carbon deposits, *viz.* FTIR, TEM, ^{13}C NMR, *etc.* [6–8]. Temperature-programmed reaction has also been useful in the identification of different forms of carbon present through reaction with different gasifying agents [9–11], *viz.*

$$C(s) + O_2(g) \rightarrow CO_2(g) \qquad \Delta H_{298K} = -393.5\,kJ\,mol^{-1} \quad (1)$$

$$C(s) + 2H_2(g) \rightarrow CH_4(g) \qquad \Delta H_{298K} = -74.5\,kJ\,mol^{-1} \quad (2)$$

$$C(s) + H_2O(g) \rightarrow CO(g) + H_2(g) \qquad \Delta H_{298K} = 131.3\,kJ\,mol^{-1} \quad (3)$$

$$C(s) + CO_2(g) \rightarrow 2CO(g) \qquad \Delta H_{298K} = 172.5\,kJ\,mol^{-1} \quad (4)$$

Syngas production from natural gas or crude oil, however, leads to increased greenhouse gas emission in the long-term. Thus, carbohydrate ($C_xH_yO_z$) reforming has attracted significant attention in recent years as it offers renewability and potential for net zero CO_2 emission during the production of syngas. Glycerol ($C_3H_8O_3$), a by-product of biodiesel manufacture with relatively low utility, is a favoured reforming substrate in the closed loop design of a biorefinery. Although the steam reforming of the oxygen-bearing molecule is expected to experience relatively lower carbon deposition compared to propane, we have observed significant organic carbon content in the used catalyst even with feed composition containing stoichiometrically excess steam [12]. In view of the paucity of information on the control and minimisation of coke with this carbon substrate, the objective of the present study was to determine the behaviour of the carbon deposition kinetics during glycerol steam reforming and the nature of the carbonaceous residue via post-reaction analysis of the used catalyst using a combination of spectroscopic and thermal analysis techniques.

* Corresponding author. Tel.: +61 2 9385 5268; fax: +61 2 9385 5966.
E-mail address: a.adesina@unsw.edu.au (A.A. Adesina).

0920-5861/$ – see front matter © 2010 Elsevier B.V. All rights reserved.
doi:10.1016/j.cattod.2010.10.040

2. Experimental

2.1. Used catalyst

Bimetallic 5 wt.%Co–10 wt.%Ni/85 wt.%Al_2O_3 catalyst was prepared and used for glycerol reforming. Metal nitrates of Co and Ni were first dissolved in nanopure water to prepare a 5 wt.%Co–10 wt.%Ni loading catalyst. The solution was then added to crushed and sieved alumina particles (Saint Gobain Nor-Pro, USA) which had been previously calcined at 873 K for 6 h. The resulting slurry was left under constant stirring for 3 h at room temperature. Impregnated catalyst was oven-dried at 403 K for 12 h and cooled to room temperature. Subsequently, the dried catalyst was sieved, ground and calcined in flowing dry air at 873 K for 4 h using a heating rate of 5 K min^{-1}. Calcined catalyst was finally sieved to 90–140 μm particle size for reaction study. Prior to actual reaction, catalyst bed (0.25 g) was activated *in situ* using H_2 at 873 K for 2 h before cooling down to the reaction temperature. Steady-state runs lasting 4 h were carried out at temperatures between 773 and 823 K and atmospheric pressure in a fixed-bed microreactor using gas-hourly space velocity, GHSV, of 5×10^4 mL g_{cat}^{-1} h^{-1}. The liquid feed (containing 30–60 wt.% glycerol solution corresponding to a steam-to-glycerol molar ratio, STGR, of 12.0–3.4) was vaporised and appropriately diluted with argon to ensure required GHSV before passage over the catalyst bed. At the end of the run, the used catalyst was cooled to room temperature under a continuous flow of argon. The carbon deposition rate was obtained via first-order forward finite difference approximation of weight change over the run period.

2.2. Catalyst characterisation

The BET surface area and pore volume were obtained from N_2 physisorption at 77 K on Quantachrome Autosorb unit. Prior to the analysis, the fresh catalyst was pre-treated under vacuum at 573 K for 3 h. X-ray diffraction (XRD) data were collected using X'Pert Pro Multi-purpose X-ray diffraction (MPD) system employing Cu Kα radiation (λ = 0.154 nm) operated at 40 mA and 45 kV. The diffractograms were analysed using X'Pert ScorePlus software. The total organic carbon content (TOC) was determined from Shimadzu TOC Analyser SM-5000A using purified compressed oxygen and analysis temperature of 1173 K. In addition, surface structure determination was performed using Nexus Nicolet FTIR spectrophotometer scanning from 650 to 4000 cm^{-1} with 4 cm^{-1} resolution. Samples were carefully mixed with KBr (FTIR grade, Sigma–Aldrich) in a mortar before measurements were taken. The coked catalysts were regenerated via different temperature-programmed treatments described in Section 2.3. Catalyst metal dispersion was evaluated using pulse H_2 chemisorption at 403 K on Micromeritics 2910 unit (Micromeritics Instruments Corp., USA). The acidic and basic properties of the catalysts were evaluated using temperature-programmed desorption (TPD) with NH_3 and CO_2 as probe gases respectively. Pulse H_2 chemisorption and TPD analyses were conducted following *in situ* reduction of the catalyst sample in H_2 at 873 K with subsequent He flushing and degassing to ensure a clean surface.

2.3. Temperature-programmed reduction (TPR) and oxidation (TPO)

Temperature-programmed methods of TPR and TPO were employed in the current study. All the carbon gasification studies were carried out in ThermoCahn TG 2121 unit. The solid sample was taken from room temperature to 973 K at a heating rate of 10 K min^{-1} followed by a holding time of 1 h in the relevant gas. For the TPR stage, 50% H_2/Ar was used while purified air was chosen for the TPO regime. All gases were dehumidified before use while coked catalyst samples were dried *in situ* at 403 K in Ar for 1 h prior to online weight analysis. The gaseous product composition from the TGA was monitored on-line via Balzers Quadstar 422 mass spectrometer.

3. Results and discussion

3.1. Influence of carbon deposition on physical properties of the catalyst

BET surface area of 166 m^2 g_{cat}^{-1} and pore volume of 0.57 cm^3 g_{cat}^{-1} were obtained for the freshly calcined catalyst. Fig. 1 demonstrates that both BET surface area and pore volume of used catalysts were smaller than the fresh specimen. In fact, the BET surface area and pore volume reduced with increasing carbon content (TOC). Furthermore, carbon deposition seemed to have more detrimental effect on the pore volume, *i.e.* approximately 50.0% reduction from the fresh catalyst (zero TOC) to catalyst with 28% TOC, compared to BET area change (20.0% reduction) in the same

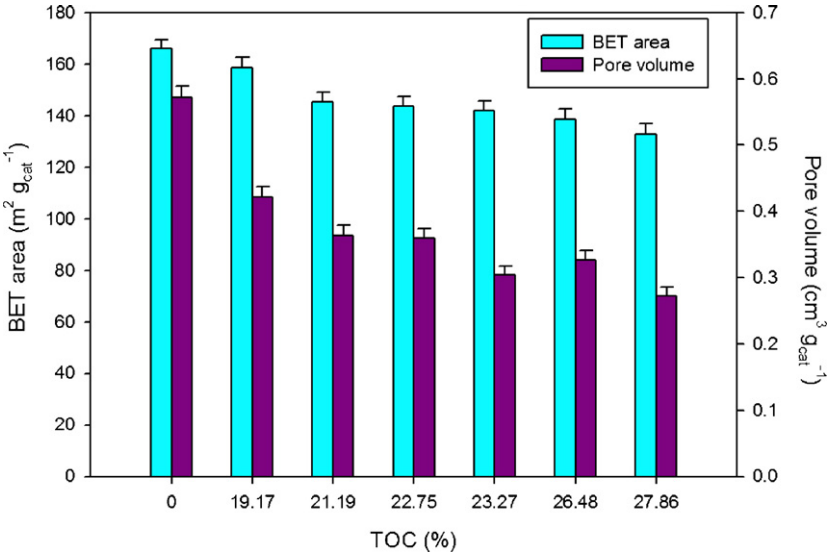

Fig. 1. Effect of TOC on BET surface area and pore volume.

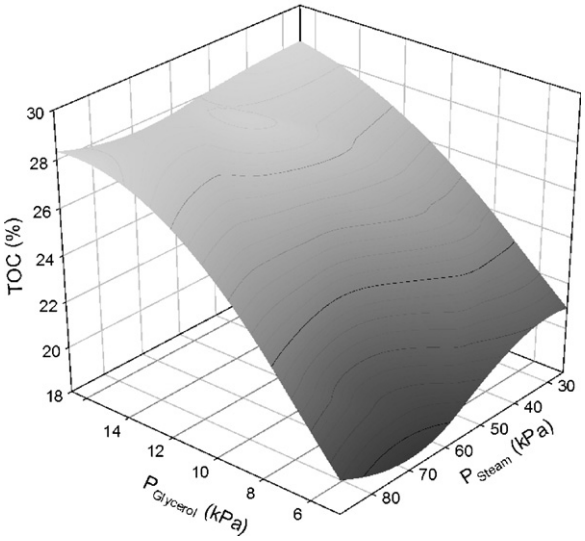

Fig. 2. TOC concentration as function of partial pressure of reactants at 823 K.

TOC range. It would seem that carbonaceous residue from glycerol adsorption blocked/narrowed the micro-channels located inside the porous alumina support rather than the pore mouths.

Fig. 2 shows the influence of partial pressure of glycerol ($P_{glycerol}$) and steam (P_{steam}) on residual TOC concentration on the used catalysts at 823 K. Higher $P_{glycerol}$ clearly enhanced carbon deposition regardless of the P_{steam} employed. Nevertheless, at a fixed $P_{glycerol}$, carbon deposition seemed somewhat inhibited by increasing P_{steam}.

3.2. Coke formation and removal

As may be seen from Fig. 3a and b, the carbon deposition rate was reasonably captured by a power–law model of the type

$$r_{deposition} = k_C P_G^{\alpha} P_W^{\beta} \quad (5)$$

with associated orders, α and β of 0.55 (glycerol) and −0.22 (steam) respectively and an activation energy value of 40.9 kJ mol^{-1}. These values are lower than those found for carbon deposition induced by propane (C_3H_8) which possesses almost identical carbon chain compared to glycerol molecule ($C_3H_8O_3$). The reaction order for propane decomposition to form carbon in the absence of steam was 0.92 while the activation energy was 205 kJ mol^{-1} as reported by Sundaram and Froment [3] while van Damme et al. [1] obtained activation energy estimate of 213 kJ mol^{-1} and first order propane decomposition with steam as diluent.

The smaller activation energy for carbon deposition during glycerol reforming may be due to the presence of the functional OH group on each of the carbon atom in the parent chain thus making it more reactive than C_3H_8 where the corresponding H (on each C atom) is less electron-withdrawing. Consequently, glycerol adsorption is expected to be stronger than propane and hence, more facile carbon deposition. Indeed, thermodynamic calculation shows that glycerol decomposition to form carbon has a larger equilibrium constant than propane dehydrogenation, namely;

$$C_3H_8O_3 \leftrightarrow 3C + 3H_2O + H_2 \qquad \Delta G_{823K} = -292.8\ \text{kJ mol}^{-1} \quad (6)$$

$$C_3H_8 \leftrightarrow 3C + 4H_2 \qquad \Delta G_{823K} = -134.0\ \text{kJ mol}^{-1} \quad (7)$$

In view of the preceding analysis and the empirical rate law, it would seem that glycerol adsorption is dissociative while steam was most likely molecularly chemisorbed, thus, a Langmuir–Hinshelwood rate expression based on a bimolecular

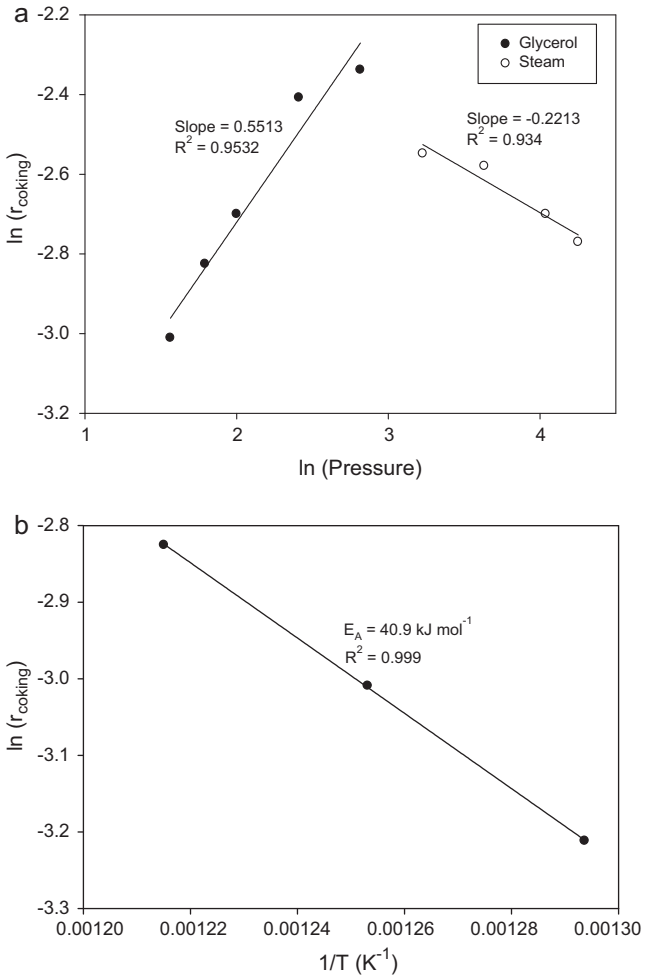

Fig. 3. Linear regression of average coking rate as function of (a) partial pressure at 823 K and (b) temperature of reaction with 30 wt.% glycerol.

rate-controlling step, may be readily derived and used to fit the carbon deposition kinetic data, thus;

$$r_{deposition} = \frac{k_{deposition} P_W \sqrt{P_G}}{\left(1 + K_W P_W + \sqrt{K_G P_G}\right)^2} \quad (8)$$

where nonlinear regression analysis gave parameter estimates, $k_{deposition}$, deposition rate constant as 4.4×10^{-1} g_{carbon} g_{cat}^{-1} h^{-1} $kPa^{-1.5}$, K_G, the adsorption constant for glycerol = 3.79×10^{-2} kPa^{-1} and K_W, the adsorption constant for steam = 6.14×10^{-5} kPa^{-1}.

3.3. Temperature-programmed removal of deposited carbon

In order to investigate the nature and location of carbon deposit, experiments were conducted with calcined pure alumina support (same particle size range, 90–140 μm, as the Co–Ni catalyst) under the same glycerol reforming conditions (30 wt.% glycerol solution, $P_{glycerol}$ = 4.78 kPa and P_{steam} = 57.00 kPa at 823 K). The coked alumina particles from this blank run as well as the used Co–Ni/Al_2O_3 catalyst were then subjected to temperature programmed reduction (with H_2) and oxidation (with air) in the manner indicated in Fig. 4a and b. As seen from Fig. 4a, there was an initial weight change due to moisture removal at 403 K followed by a rather gentle weight drop in the presence of H_2 which seemed completed after about 5000 s. However, during the subsequent TPO, the used

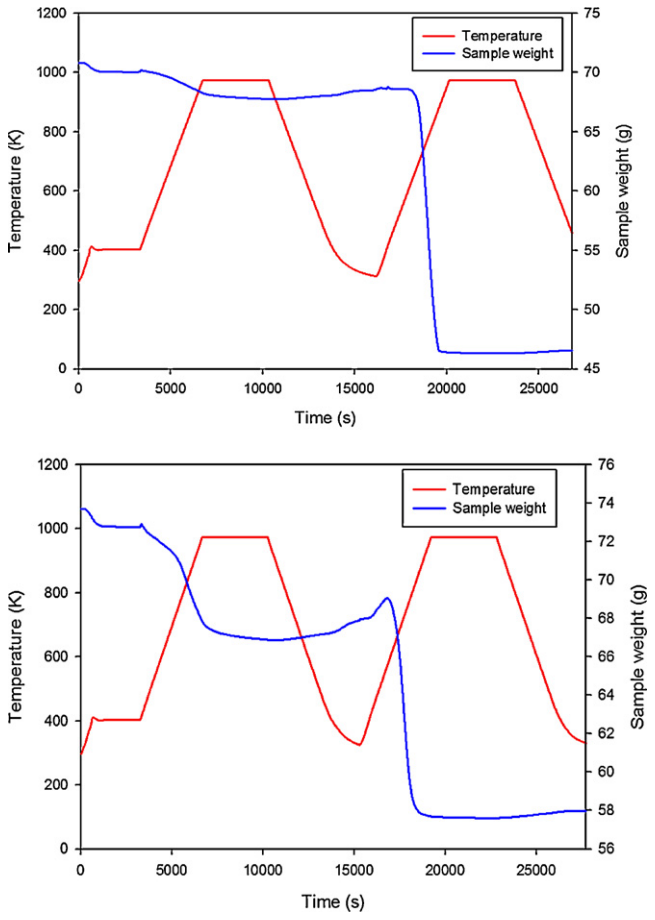

Fig. 4. (a) Calcined alumina support only and (b) Co–Ni/Al_2O_3 after glycerol steam reforming at 823 K. Heating rate during TPR and TPO regimes was 10 K min^{-1}.

calcined alumina support experienced another sharp weight drop which quickly levelled out. This would indicate that there was still significant carbon residue on the solid at the end of the previous H_2-TPR. The relatively little weight drop during TPR showed that the left-over carbonaceous pool was essentially inert to H_2 but readily gasified by O_2 (as seen during TPO). The smaller carbon deposit reactive with only H_2 was about 8% of the total carbon on the alumina while the larger pool removed during TPO was about 92%. Since the calcined alumina contained weak acid sites [12], carbon deposition may have taken place via glycerol adsorption on these acid centres. Fig. 5 (curve a), the derivative weight plot for coked calcined alumina has a single peak at 590 K for the TPR. The corresponding transient gas phase composition (from mass spectrometer) shown in Fig. 6a revealed the evolution of CH_4 and H_2O indicating that the surface carbonaceous layer contained, C, H and O atoms consistent with a glycerol adsorbate species. The derivative weight profile for the TPO regime (curve c of Fig. 5) is characterised by a small peak at 650 K and a more prominent, broader peak centred at 780 K. The associated gas phase (cf. Fig. 6a) has CO_2 as the key component with small amounts of H_2O and CO and no detectable CH_4.

The Co–Ni/Al_2O_3 catalyst, however, appeared to experience greater carbon deposition probably due to the presence and higher concentration of both weak and strong acid sites [12]. As may be seen from Fig. 4b, there was substantially higher weight loss during TPR than in the calcined alumina. Fig. 5 (curve b) shows that this carbon residue has a complex composition indicated by a smaller peak at 570 K and a more distinctive peak located between 700 and 973 K. This is also corroborated by the associated gas phase composition profile in Fig. 6b where a strong CH_4 peak is evident. This carbon pool was about 40% of the total carbon reservoir on the catalyst surface. The remaining 60% was reactive with O_2 during the TPO phase. Fig. 5 (curve d) shows a diminutive peak at 630 K and a

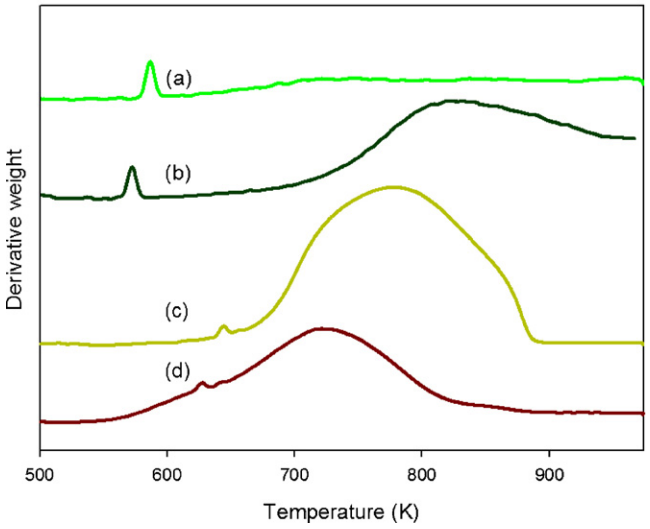

Fig. 5. Derivative weight profiles for TPR–TPO with (a) TPR on used alumina, (b) TPR on used catalyst, (c) TPO on used alumina and (d) TPO on used catalyst.

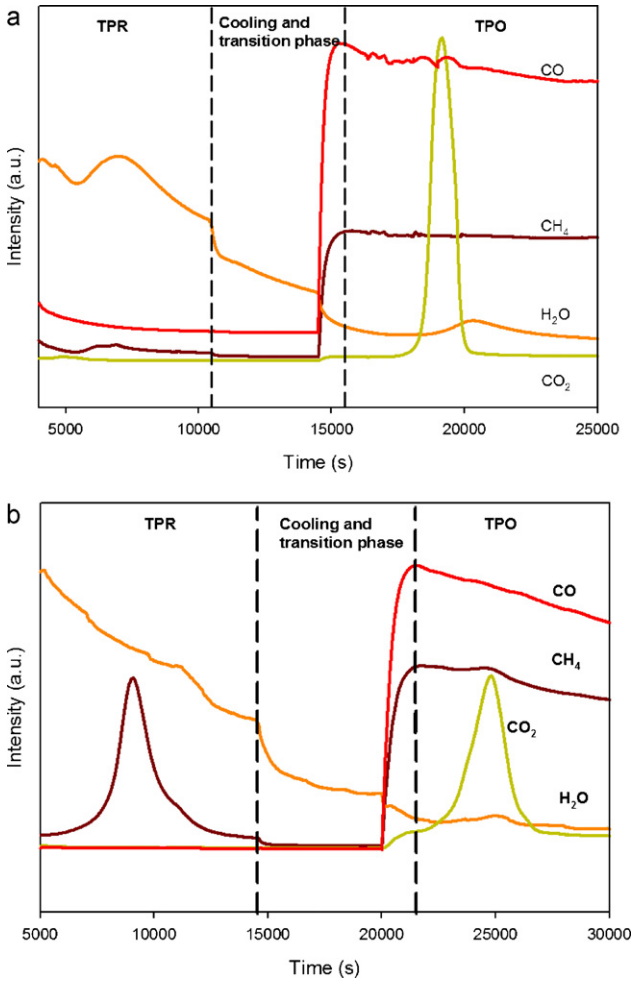

Fig. 6. Mass spectrometer profiles showing product formation from carbon gasification on (a) used alumina and (b) used Co–Ni catalyst.

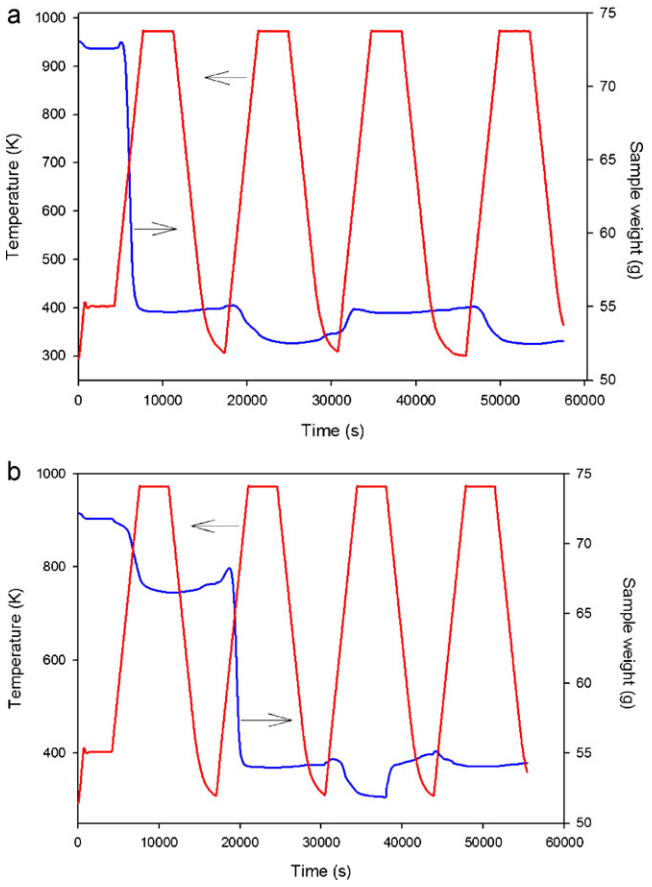

Fig. 7. Derivatives weight changes of coked catalysts employing (a) TPO–TPR–TPO–TPR cycles and (b) TPR–TPO–TPR–TPO cycles.

bigger, broader peak centred at 720 K. Mass spectrometry profiles show CO_2 and H_2O as the identifiable ingredients in the effluent gas stream. The higher oxidation temperature peaks on the alumina support is indicative of a less reactive carbon deposit compared to the residue on the Co–Ni/Al_2O_3 catalyst.

The carbon pool reactive with H_2 may be attributed to atomic carbonaceous deposit (C_α) since its removal in H_2 is accompanied by CH_4 evolution in the gas phase as seen in the mass spectrometric composition analysis (cf. Fig. 6). As a result, we inferred that the H_2-resistant carbon deposit was primarily polymeric species and empirical composition analysis (using weight changes during the TPR and TPO runs) revealed a C:H ratio of 6:1 for this carbon species and a 1:1 for the C_α pool. Based on the solid acid properties provided in Table 2, it would seem that the polymeric carbon species were located on the weak acid sites while the C_α atomic carbon would be on the strong acid centres.

3.4. Catalyst regeneration

The coked catalyst was subjected to two types of temperature-programmed treatment (cf. Fig. 7) in order to evaluate the recoverability of the physicochemical properties of the freshly calcined catalyst.

The results from TPO–TPR–TPO–TPR cycle (cf. Fig. 7a) revealed a complete carbon burn-off on the coked catalyst. This is evidenced by the precipitous drop in the weight of the catalyst sample during the TPO regime. The smaller weight drop in the subsequent step (TPR), marked the reduction of metal oxides in the sample. In the next step (TPO), oxidation of reduced metals took place and the resulting weight rise attained the level registered during the first TPO phase. Howbeit, the second and final TPR step returned the sample weight back to the level seen in the first TPR step.

The second scheme (cf. Fig. 7b), TPR–TPO–TPR–TPO cycle, showed that H_2 was not as effective as O_2 in carbon gasification based on the comparison of weight drops from the first TPO regime of Fig. 7a and the first TPR step in Fig. 7b. As expected, weight decrease during the first TPO in Fig. 7b was higher than in the preceding TPR. The second TPR regime (of the TPR–TPO–TPR–TPO cycle) essentially reduced the metal oxide phases from the prior TPO step (somewhat below that seen during the equivalent TPR in Fig. 7a). However, the final TPO regime returned the weight to its level during the previous TPO. The results from these two different temperature-programmed schemes underscore the total recoverability of surface physicochemical properties of coked catalyst from glycerol steam reforming and hence, possible innovative forced temperature or composition cycling for the reactor operation to improve catalyst longevity [11]. It requires the second step which employed air as reactant gas to achieve complete burn-off of carbon. The reversibility of the surface properties of coked catalyst was evidenced once again from the second TPR and TPO steps.

The regenerated catalysts from both temperature-programmed treatments were subjected to physicochemical characterisation. Table 1 shows the physical properties obtained from the analysis done on Quantachrome Autosorb unit.

The data in Table 1 suggest that the removal of carbon from the coked catalyst via any of the thermal treatments is accompanied by more than 90% recovery of its nascent structural characteristics (BET area and pore volume). The relatively identical pore volume values for both sets of regenerated catalysts indicate that there was no pore blockage due to carbon deposition, in agreement with the TGA results shown earlier. The small reduction in BET area may be symptomatic of marginal sintering effect, most likely due to crystallite growth promoted by higher regeneration treatment (973 K) as opposed to fresh catalyst calcined at 873 K. It would, however, seem that regeneration using the TPO–TPR–TPO–TPR scheme produced a slightly superior rejuvenated catalyst. As a result, further characterisation was done on the catalyst reconditioned under this scheme with properties as shown in Table 2. Regenerated catalyst showed slightly lower metal surface area (0.69 $m^2\ g_{cat}^{-1}$) and larger active particle diameter compared to fresh catalyst (0.74 $m^2\ g_{cat}^{-1}$), indicative of possible minor particle sintering. Significantly, comparison of other intrinsic catalyst properties such as acid and basic properties (desorption energy and concentration) indicated that these properties were nearly recovered after the regeneration process. The small difference observed could be due to the different regeneration and catalyst calcination temperatures as aforementioned.

Table 1
Physical properties of regenerated catalysts.

Treatment type	BET area ($m^2\ g_{cat}^{-1}$)	Pore volume ($cm^3\ g_{cat}^{-1}$)	Pore diameter (nm)
TPR–TPO–TPR–TPO	151.6	0.54	141.9
TPO–TPR–TPO–TPR	157.0	0.56	141.3
Freshly calcined Co–Ni/Al_2O_3 catalyst	166	0.57	130.7
Calcined Al_2O_3 support	210	0.69	130.6

Table 2
Physicochemical properties of regenerated catalyst after temperature-programmed heat treatment.

Properties	Type of sites	Regenerated catalyst	Fresh catalyst	Calcined support
Dispersion (%)		0.69	0.74	N/A
Metal surface area ($m^2\ g_{cat}^{-1}$)		0.69	0.74	N/A
Active particle diameter (nm)		146.5	136.0	N/A
NH_3 desorption energy, ΔH_{NH_3} ($kJ\ mol^{-1}$)	Weak site	37.00	35.46	68.90
	Strong site	82.80	87.30	N/A
CO_2 desorption energy, ΔH_{CO_2} ($kJ\ mol^{-1}$)	Weak site	63.54	62.42	63.20
	Strong site	53.52	55.97	68.40
Acid concentration ($\mu mol\ m^{-2}$)	Weak site	1.39	1.50	2.13
	Strong site	2.76	2.90	N/A
Basic concentration ($\mu mol\ m^{-2}$)	Weak site	0.14	0.21	0.14
	Strong site	0.39	0.42	0.32
Acid:basic sites ratio	Weak site	9.92	7.33	15.40
	Strong site	7.07	6.98	N/A

3.5. FTIR and XRD analyses

Fig. 8 shows the FTIR spectra obtained for four different catalyst specimens. Sample *A* was the freshly calcined catalyst, Sample *B*, the calcined alumina support employed in the blank glycerol steam reforming run, Specimen *C* represented the used catalyst obtained from glycerol reforming while Sample *D* was the regenerated Co–Ni/Al_2O_3 catalyst. Clearly, samples *A* and *D* exhibited parallel spectra features, indicating similarity in the surface chemical composition of both samples. Additionally, it confirmed that the regenerated sample was free from any carbon residue. Both samples *B* and *C* yielded FTIR spectra implicating the existence of hydrocarbon species on catalyst surface. In particular, the band at 1015 cm^{-1} is consistent with C–O and C–C stretch mode while the 1650 cm^{-1} band may be assigned to the C=C bond. A weak signal at 2850 cm^{-1} may be attributed to the presence of C–H bond while the broad signal at 3500 cm^{-1} is a well known signal for the O–H group. The presence of Al^{3+} species is reflected in the signals located between 2262 and 2446 cm^{-1}.

Fig. 9 shows the comparison of X-ray diffraction patterns for the same four solid samples examined in Fig. 8. The carbon peak detected at $2\theta = 26^\circ$ on both used calcined alumina support and catalyst is evidence that the deposited carbon has a crystalline (graphitic) rather than an amorphous nature [13]. Importantly, the XRD pattern for the regenerated Co–Ni catalyst did not show any carbon peak, consistent with temperature-programmed profiles shown earlier. Moreover, the presence of metal aluminate peaks ($2\theta = 38^\circ$ and 45°) in used and regenerated Co–Ni samples confirms

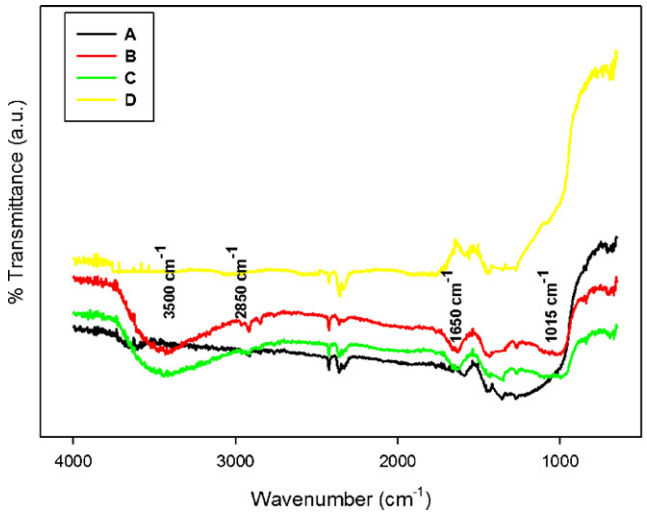

Fig. 8. FTIR spectra for (A) freshly calcined catalyst, (B) used alumina support, (C) used Co–Ni catalyst for glycerol reforming and (D) regenerated Co–Ni catalyst.

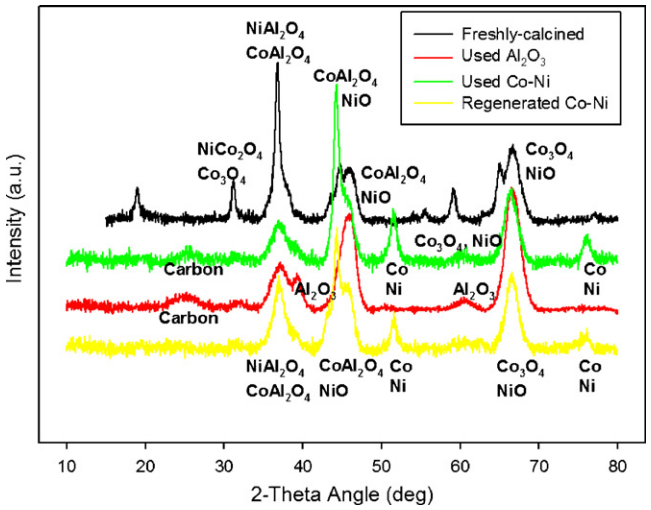

Fig. 9. X-ray diffractograms of freshly calcined catalyst, used catalyst, regenerated catalyst and used alumina support only.

that this phase was not completely reduced under the conditions employed in this study. Significantly, the Co and Ni metallic phases were seen ($2\theta = 52^\circ$ and 77°) in these two specimens, suggesting that under the steam reforming conditions the initially reduced catalyst was not completely re-oxidized possibly due to the reducing effect of H_2 and CO product species. Moreover, partially separated peaks at 2θ values between 65° and 68° represents Co_3O_4 and NiO phases in the calcined, used and regenerated catalysts.

4. Conclusions

Carbon deposition on bimetallic Co–Ni/Al_2O_3 catalyst during steam reforming of glycerol was possible even with feed containing stoichiometrically excess steam. However, steam has a mild inhibition effect on the deposition rate as indicated by a negative order (–0.22). Indeed, a Langmuir–Hinshelwood kinetic model based on dissociative glycerol adsorption and molecular chemisorption of steam adequately described the carbon deposition rate. BET area and pore volume of the catalyst also decreased with increasing TOC values (arising from the catalyst history). The latter was also correlated with the concentration of acid sites (both weak and strong) on both catalyst and calcined alumina support. Thermogravimetric analysis (TPR and TPO) showed that there are two types of surface carbonaceous species. A relatively small residue reactive with both H_2 and O_2 as well as a bigger reservoir which could only be gasified with O_2. Mass spectrometric analysis of the effluent gas stream from the TGA unit confirmed CH_4 and H_2O as the

key components during H_2-TPR while CO_2 and H_2O were produced in the TPO regime. FTIR examination of the solid samples also revealed the presence of C–O, C–C, C–H and O–H bonds consistent with the presence of glycerol adsorbate while the C=C stretch mode at 1650 cm^{-1} is indicative of surface olefinic species attributed to dehydropolycondensation of C_yH_{1-y} fragments present in the bigger carbon pool. Catalyst regenerative runs using TPR–TPO–TPR–TPO and TPO–TPR–TPO–TPR cycles demonstrated that the carbon residue can be completely removed to restore the catalyst to its nascent state since the physicochemical properties of the rejuvenated catalysts are essentially the same as those of the fresh Co–Ni/Al_2O_3 sample. The bulk phase structural characteristics were also similar as verified from X-ray diffractograms.

Acknowledgements

The authors are grateful to the Australian Research Council for financial support. CKC appreciates the University International Postgraduate Award (UIPA) from the University of New South Wales, while SYF is a recipient of the Australian Postgraduate Award (APA).

References

[1] P.S. Van Damme, S. Narayanan, G.F. Froment, AIChE J. 21 (1975) 1065.
[2] Y.T. Shah, E.B. Stuart, K.D. Sheth, Ind. Eng. Chem., Process Des. Dev. 15 (1976) 518.
[3] K.M. Sundaram, G.F. Froment, Chem. Eng. Sci. 34 (1979) 635.
[4] C.H. Bartholomew, M.V. Strasburg, H.-Y. Hsieh, Appl. Catal. 36 (1988) 147.
[5] J. Gascón, C. Téllez, J. Herguido, M. Menéndez, Appl. Catal. A: Gen. 248 (2003) 105.
[6] F. Diez, B.C. Gates, J.T. Miller, D.J. Sajkowski, S.G. Kukes, Ind. Eng. Chem. Res. 29 (1990) 1999.
[7] C.L. Pieck, E. Jablonski, J.M. Parera, R. Frety, F. Lefebvre, Ind. Eng. Chem. Res. 31 (1992) 1017.
[8] K.M. Hardiman, C.G. Cooper, A.A. Adesina, R. Lange, Chem. Eng. Sci. 61 (2006) 2565.
[9] C.A. Querini, S.C. Fung, Appl. Catal. A: Gen. 117 (1994) 53.
[10] B. Sánchez, M.S. Gross, B. Dalla Costa, C.A. Querini, Appl. Catal. A: Gen. 364 (2009) 35.
[11] F. Alenazey, C.G. Cooper, C.B. Dave, S.S.E.H. Elnashaie, A.A. Susu, A.A. Adesina, Catal. Commun. 10 (2009) 406.
[12] C.K. Cheng, S.Y. Foo, A.A. Adesina, Ind. Eng. Chem. Res., doi:10.1021/ie100462t, in press.
[13] K.M. Hardiman, T.T. Ying, A.A. Adesina, E.M. Kennedy, B.Z. Dlugogorski, Chem. Eng. J. 102 (2004) 119.